

ZACK: Zero-Overhead LLM Inference Acceleration via Dimensionality Compression of the Key-Value Cache

Zeyu Zhang
University of Virginia

Haiying Shen
University of Virginia

Abstract

In large-language models, memory constraints in the Key-Value Cache (KVC) pose a challenge during inference. In this work, we propose ZACK, the first KV dimensionality compression system that achieves *zero-overhead* compression and decompression and also reduces attention computation time. It complements and can be combined with eviction-based and quantization-based methods to further enhance KV compression. Moreover, ZACK employs adaptive compression, tailoring KV compression rates across heads and layers based on their contributions to inference to maximize overall compression while maintaining an accuracy loss constraint. Additionally, ZACK enhances the self-attention kernel to balance the uneven workloads caused by the adaptive compression approach to further reduce attention computation latency. Comprehensive experiments demonstrate that when combined with ZACK, state-of-the-art eviction-based and quantization-based methods for KV compression further reduce KV size by up to 68%, Time-To-First-Token (TTFT) by up to 44%, and Time-Between-Tokens (TBT) by up to 55% and achieve up to $1.72\times$ throughput under the same latency, while maintaining 99% of the baseline accuracy. We open-sourced the code.

1 Introduction

Generative large language models (LLMs) [1–6] have transformed natural language processing (NLP), showcasing remarkable performance across various tasks like text completion [7], dialogue generation [8], code synthesis [9], language translation [10], text summarization [11–13], and document classification [14, 15]. The LLM models are primarily inspired by the transformer architecture [16], which employs self-attention to capture long-range dependencies in sequences.

During LLM inference, text generation starts with providing a prompt. LLM generates the first token via prompt processing (a.k.a., prefill), followed by text generation (a.k.a., decode) to generate new tokens. LLMs typically consist of multiple transformer layers, where each layer receives an embedding matrix E for the entire input. These embeddings are

projected to produce Query (Q), Key (K), and Value (V) components for each token, serving as inputs to the self-attention layer. We use italicized Q , K , and V to represent their respective matrices. The KV values of newly generated tokens are stored in KVC to avoid redundant computations. During token generation, the KV values of previous tokens are fetched from the KVC and fed into the attention layer. The resulting self-attention output guides token generation.

The primary challenge of LLM inference is memory constraints within KVC, which limits GPU utilization and consequently decreases throughput. To address it, various KV compression methods have been proposed and they can be divided into two main categories: token eviction methods [17–26] and quantization methods [27–31]. Token eviction methods remove the KV values of unimportant tokens that have minimal impact on the inference results. Quantization methods compress KV values by reducing the bit width of each element in the KV matrix from a higher bit width (e.g., float16) to a lower bit width (e.g., 4-bit, 2-bit).

In this paper, we propose a novel KV compression approach by reducing the *hidden dimension* of KV, which can complement the token eviction and quantization methods to further reduce KV size. Inspired by the use of Singular Value Decomposition (SVD) [32] in NLP to reduce the dimensionality of word embeddings post-training, we explore leveraging SVD to compress the dimensionality of KV data. We first demonstrate that it is feasible to use SVD for KV compression (§3.1). Specifically, we use SVD to compute the rotation matrices R for K and V , respectively. By rotating the K and V vectors of each token using R , the resulting KV vectors exhibit numerous dimensions with low-magnitude components, which can be removed to reduce the KV size. To decompress the data, we simply apply the inverse of the rotation matrix R to rotate the vectors back to their original orientations.

However, directly using SVD to compress KV introduces significant overhead (§3.2). The online computation of the rotation matrix R accounts for 23.7% of Job Completion Time (JCT), compressing KV during prefill takes up 5.9% of JCT, and decompressing KV during decode occupies 39.8% of

JCT. To tackle the issue, we propose ZACK, Zero-overhead LLM inference Acceleration via Dimensionality Compression of the KVC, which not only eliminates the compression and decompression time overhead in KV dimensionality reduction but also reduces attention computation time. Note that ZACK is novel in its ability to **eliminate** the overhead entirely, reducing it to zero rather than merely decreasing it. ZACK comprises three key components as below.

SVD-based zero-overhead KV compression. We establish three lemmas indicating conditions to eliminate 1) compression time, 2) decompression time, and 3) time to compute rotation matrix R . We find that SVD meets these conditions. To achieve 1), we integrate R into model parameters to conceal KV compression into model operations, which also reduces the KV generation time. To achieve 2), ZACK compresses KV and Q, pairs Q with K and V with model parameters, and uses the matrix multiplication of compressed matrices to directly approximate the result obtained by multiplying their uncompressed counterparts during model operations. This also reduces the attention computation time. To achieve 3), ZACK computes R offline using a synthetic dataset with sufficient distinct tokens constructed from linguistically coherent sentences.

Adaptive compression rate. Model layers contribute differently to the output [16], as do the attention heads within each layer [18]. Thus, ZACK applies different compression rates to K and V in different heads and layers to maximize the overall KV compression rate given an accuracy constraint. These compression rates are determined by the magnitude of the components in each dimension of the rotated KV vectors.

Self-attention kernel enhancement for adaptive compression rate. The different compression rates on the hidden dimensions of QKV in ZACK can lead to imbalanced execution times across a GPU’s Stream-Multiprocessors (SM). Thus, ZACK balances the uneven workloads across SMs for self-attention in the prefill and decode stages, respectively, to further reduce self-attention computation latency.

In summary, our work has the following contributions:

- We provide geometric explanations and conduct extensive experiments with numerous state-of-the-art models and complex-task datasets to demonstrate the rationality and feasibility of ZACK’s design principles.
- We propose ZACK, the first KV dimensionality compression system without the overhead of compression and decompression. It can complement existing token eviction based and quantization based KV compression methods, and also reduce attention computation time.
- Comprehensive experiments demonstrate that compared to the baseline without compression, ZACK achieves up to a 0.69 KV compression rate, reduces TTFT by up to 48% and TBT by up to 61%, and delivers up to $2.24\times$ throughput under the same latency, while maintaining 99% of the baseline accuracy. When combined with ZACK, state-of-the-art eviction-based and quantization-based methods for KV com-

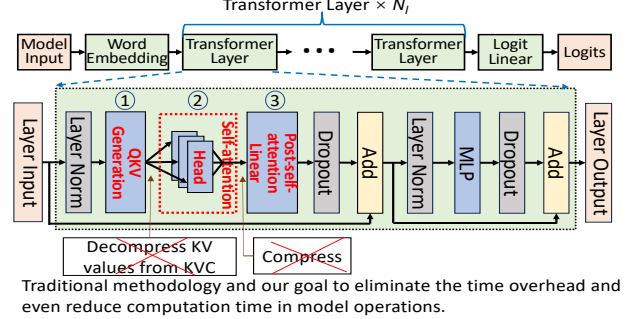


Figure 1: The overview of a typical transformer layer.

pression further reduce KV size by up to 68%, TTFT by up to 44%, and TBT by up to 55% and achieve up to $1.72\times$ throughput under the same latency, while maintaining 99% of the baseline accuracy.

We open-sourced the code of ZACK [33].

2 Background

2.1 Attention Mechanism of Transformers

Fig. 1 shows a typical transformer-based generative LLM with identical transformer layers. Each layer mainly consists of a Multi-Layer Perceptron (MLP) and a multi-head attention mechanism, which encompasses three main parts, as highlighted in red. The mechanism enables the model to evaluate the interdependencies among all tokens in a sentence across different aspects represented by different attention heads. Within head h , each token (represented by token embedding $e \in E$) undergoes transformation into a query $q^h \in Q^h$, a key $k^h \in K^h$, and a value $v^h \in V^h$ through QKV generation (①):

$$Q^h = EW_Q^h, \quad K^h = EW_K^h, \quad V^h = EW_V^h, \quad (1)$$

where W_Q^h , W_K^h , and W_V^h are the parameter matrices. The self-attention layer (②) computes the output in each head h :

$$O^h = \text{Softmax}\left(\frac{Q^h(K^h)^T}{\sqrt{d_h}}\right)V^h = P^hV^h. \quad (2)$$

The softmax function operates row-wise on the input matrix $[a_{i,j}]$ as follows:

$$\frac{\exp(a_{i,j})}{\sum_{k=1}^{t_i} \exp(a_{i,k})}, \quad (3)$$

where t_i is the index of the token on row i . In prefill, Q^h , K^h , and V^h are derived from the input sequence. In decode, Q^h is obtained from the input token, while K^h and V^h of all previous tokens are retrieved from the KVC. The outputs from all heads are concatenated together along the head dimension to form the self-attention output O . In the post-self-attention linear layer (③), this output is then transformed by the parameter matrix W_L to produce the linear layer output:

$$O_L = [O^1, O^2, \dots, O^{N_h}]W_L = OW_L. \quad (4)$$

Table 1 lists the primary notations used in the paper. We define *attention* as the module comprising ①, ②, and ③, with ② specifically referred to as *self-attention*.

2.2 Matrix Multiplication and Redundancy in Vector Representation

The essence of matrix multiplication is linear transformation, which can be understood as transforming one set of vectors into another set through a linear transformation.

$$\begin{bmatrix} a_0 & a_1 \\ b_0 & b_1 \end{bmatrix} \times \begin{bmatrix} m_{0,0} & m_{0,1} \\ m_{1,0} & m_{1,1} \end{bmatrix} = \begin{bmatrix} a'_0 & a'_1 \\ b'_0 & b'_1 \end{bmatrix} \quad (5)$$

Eq. (5) represents transforming vectors $\langle a_0, a_1 \rangle$ and $\langle b_0, b_1 \rangle$ to vectors $\langle a'_0, a'_1 \rangle$ and $\langle b'_0, b'_1 \rangle$ through a matrix $[m_{i,j}]$. For QKV generation, E is a set of token embedding vectors. The model parameter (e.g., W_Q^h) is a transformation matrix. The essence of QKV generation is transforming token embedding vectors into other vectors (e.g., Q^h).

After a linear transformation, the resulting vectors may have a large component in a direction in space and a substantially small component in some other directions. Fig. 2 shows that after the matrix transformation in Step ①, vectors a' , b' , c' , and d' all lie on the line $y = x$. The components of a' , b' , c' , and d' along the $y = x$ direction are large, while those along the orthogonal direction ($y = -x$) are zero. To represent each vector, we need both the x - and y -axis component values. However, if in Step ② in Fig. 2, we apply a rotation matrix R to rotate a' , b' , c' , and d' 45° clockwise, aligning the $y = -x$ direction with the y -axis, the rotated vectors a'' , b'' , c'' , and d'' will have zero components along the y -axis and large components along the x -axis. This way, we can ignore the y -axis and use the x -axis components to represent a'' , b'' , c'' , and d'' , reducing the number of dimensions while preserving the relationships among a' , b' , c' , and d' . This method of rotating a set of vectors to align certain low-component directions with specific coordinate axes and then removing those axes is often used in NLP for dimensionality reduction of data. The approach to finding the rotation matrix R is SVD [32].

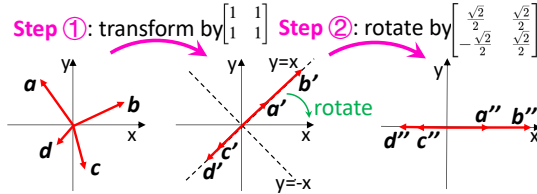


Figure 2: Linear transformation and vector rotation.

2.3 Singular Value Decomposition

SVD is widely used to reduce data dimensionality with low or even zero loss. Figure 3: SVD for data compression. Given a matrix A where each row represents an item's vector to be compressed, A can be decomposed into $A = U\Sigma R^T$. U and R are rotation matrices, while Σ is a diagonal matrix filled with zeros except for non-negative singular values sorted in descending order along the diagonal. This decomposition,

d	Model dimension size	N_h	The number of heads
N_l	The number of layers	d_h	Head dimension size ($= d/N_h$)
E	Token embeddings	Q	Query matrix
K	Key matrix	V	Value matrix
R	Rotation matrix	p	Compression rate
W	Parameter matrix	s	Sequence length

Table 1: Notations used in the paper.

solvable using an SVD solver [34], has a unique solution. Singular values quantify the magnitude of vectors' components after rotation by R . Consequently, each row of $A^R = AR$ is a rotated vector with elements decreasing from left to right, and the right p fraction of the columns of A^R can be discarded with minimal impact on vector relationships. This creates a compressed matrix A^{R_p} , with R_p as the compression matrix, as depicted in Fig. 3. To decompress the data, we only need to use the inverse of R , equivalent to R^T for rotation matrices, to rotate the compressed vectors back to their original orientation. Since the deleted dimensions can be considered zero-valued, we do not require the full R^T for decompression; instead, R_p^T suffices.

3 Experimental Analysis

KV vectors can be viewed as parameter-matrix-transformed vectors after Step ① in Fig. 2. Our goal is to determine if we can rotate the KV vectors and remove dimensions with low-magnitude components in Step ② in Fig. 2 to compress KV while preserving the original information as much as possible. In this section, we address two key questions.

- First, do the KV vectors have low-magnitude components, making KV data compression feasible?
- Second, if low-magnitude components exist in the KV vectors, what is the computational cost of compressing and decompressing KV vectors during model inference?

Llama-3.1	8B, no TP and PP	Yi	9B, no TP and PP
	70B, TP=4		34B, TP=4
Mistral-v0.3	7B, no TP and PP	Phi-3	14B, no TP and PP
Falcon	180B, TP=4, PP=2		

Table 2: Model size and TP/PP size.

Trace	Input length			Output length		
	avg	min	max	avg	min	max
IMDb classification [35]	315	106	821	37	16	87
arXiv summarization [36]	6.3K	1.6K	14.1K	243	29	464
Cocktail for IR [37]	16.2K	9.4K	28.8K	159	44	246
HumanEval [38]	204	75	697	139	11	552

Table 3: Trace properties.

In the experimental analysis, unless otherwise specified, we utilized the following settings. We used the state-of-the-art models: Meta Llama-3.1 [39], 01-ai Yi [40], Mistral AI Mistral-v0.3 [41], Microsoft Phi-3 [42], and TII Falcon [43]. Table 2 lists the model size and Tensor Parallelism (TP) and Pipeline Parallelism (PP) size, following the setting in [44, 45]. We used the datasets listed in Table 3. IMDb includes 27 genres of movies, TV shows, etc., collected on the Internet. It is operated by IMDb.com, Inc., a subsidiary of Amazon. The

arXiv summarization has a collection of scientific publications and their summaries on arXiv.org [36]. Information Retrieval (IR) is the process of retrieving relevant content from vast amounts of information based on a user query. The Cocktail is a benchmark for IR, including 8 different IR tasks such as question answering, fact checking, etc. HumanEval evaluates the performance of code completion, including 164 programming problems. Cocktail contains no sequences shorter than Falcon 180B’s 2K context window length, which is indicated as N/A in the paper.

We employed four AWS p4de.24xlarge instances [46] located in four nodes. Each instance is equipped with 8 NVIDIA A100 GPUs (each with 80 GiB memory), 96 vCPUs, and 1152 GiB host memory, connected with a 400 Gbps network. As in [47], we executed 16 concurrent clients to dispatch requests from a single dataset. We built our system atop vLLM [48] and scheduled each request to a vLLM instance (which holds one model replica) that has the shortest queue length [49]. By default, the request rate is set to the maximum processing capacity without increasing queuing time, based on a Poisson distribution.

3.1 Feasibility for Compressing the Dimensionality of KV Vectors

We begin by addressing the first question. Fig. 4 illustrates how we use SVD, as introduced in §2.3, to rotate a set of K or V vectors. First, we arrange all K or V vectors row-wise to form a matrix A in each head. Then, we apply SVD to decompose A into $U\Sigma R^T$ (1). The singular values are located on the diagonal of Σ . R serves as the rotation matrix we seek to rotate the vectors. In (2), the green rotated vectors obtained through R are still arranged row-wise, and each rotated vector has elements arranged in descending order from left to right, a consequence of the singular values’ arrangement in Σ . In other words, the magnitude of the singular values on the diagonal determines the relative size of each element in the rotated vectors. The larger the singular value, the greater the element value in the corresponding dimension, and vice versa. If we want to remove the smallest N elements from each rotated vector, we simply need to delete the rightmost N columns of R in (2), as introduced in §2.3.

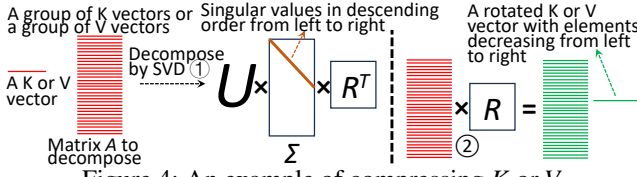


Figure 4: An example of compressing K or V.

For each model and dataset, we collected all K and V vectors for every token, head, and layer. Since the processing steps for K and V vectors are identical, we use the K vectors as an example for illustration. For all K vectors collected within each head, we performed SVD decomposition as shown in Fig. 4 to obtain singular values

$g_K^{i,h,l}$ for head dimension $i \in [0, d_h - 1]$, head h , and layer l . The head dimension size d_h is typically 128. Given a model and a dataset, we compute the average singular value $\bar{g}_K^i = \frac{1}{N_h N_l} \sum_{h=1}^{N_h} \sum_{l=1}^{N_l} g_K^{i,h,l}$ for head dimension i by averaging the singular values across all heads. Fig. 5 shows the average singular value for each head dimension for K vectors and V vectors with different models and datasets. The curves of different models are almost overlapped. For K vectors and V vectors of any model with any dataset, we observe that the average singular values are significantly large in the initial dimensions on the far left, and those in the remaining dimensions are extremely small. This indicates that K vectors and V vectors have many directions with low-magnitude components, making dimensionality compression feasible.

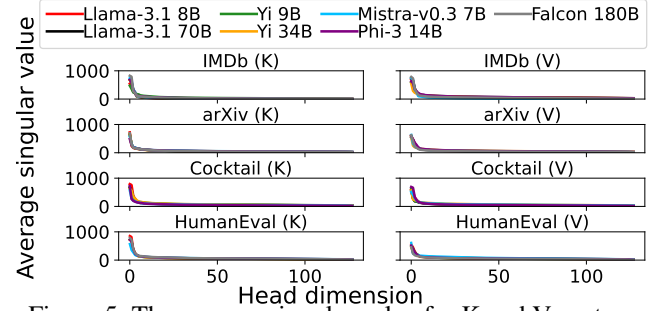


Figure 5: The average singular value for K and V vectors.

Observation 1 KV vectors have many directions with low-magnitude components in space, making it possible to use SVD to compress KV dimensionality losslessly.

3.2 Overhead of KV Dimensionality Compression and Decompression

We then address the second question. We implemented a simple strawman method atop vLLM. In prefill, the strawman method performs SVD decomposition on the K vectors and V vectors for each head, obtaining a rotation matrix R for K and V , respectively. The strawman then uses these rotation matrices to rotate the corresponding K and V vectors, removes the rightmost 50% of dimensions from the rotated vectors, and stores the compressed vectors in KVC. In decode, at each iteration, the strawman retrieves the K and V vectors from KVC and decompresses them by applying the inverse rotation R^T . The K and V vectors generated from the input token are also rotated and compressed using their respective R before being stored in KVC.

Fig. 6 presents the average percentage of each component of JCT among all requests given a dataset and a model. We observe that finding rotation matrix R through SVD decomposition takes 9.4%-23.7% of JCT. Compressing K and V vectors by their respective rotation matrix R in prefill takes 3.1%-5.9% of JCT, which involves matrix multiplication between KV vectors and their R with a small shape of (d_h, d_h) , typically (128, 128). In decode, decompressing K and V data accounts for 22.4%-39.8% of the JCT. This involves multiplying the compressed K and V vectors with their respective

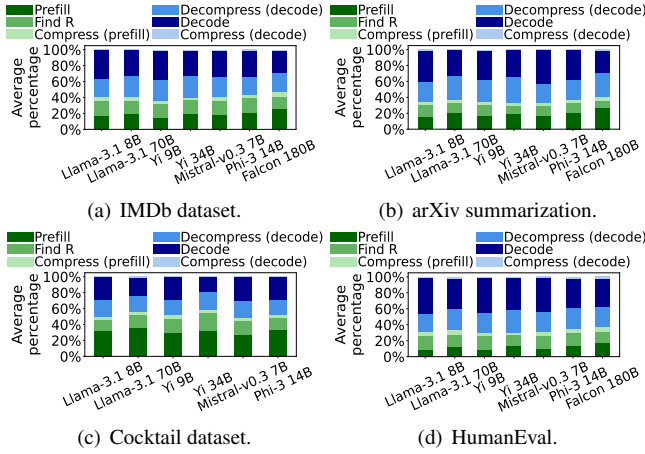


Figure 6: The JCT decomposition for the strawman method.

R^T to perform inverse rotation. Since each decode iteration only requires compressing the KV vectors of a single input token to be stored in KVC, this overhead is relatively small, accounting for only 0.6%-1.3% of the JCT.

Observation 2 *Directly using SVD for KV compression incurs significant overhead: computing R consumes 9.4%-23.7% of JCT, KV compression in prefill takes 3.1%-5.9%, and KV decompression in decode accounts for 22.4%-39.8%, with negligible time spent on KV compression in decode.*

4 Rationale of the Design of ZACK

Observation 1 (O1) demonstrates the feasibility of SVD for KV dimensionality reduction. O2 underscores the importance of minimizing compression overhead. Therefore, our goal is to design a system with minimal or zero additional overhead for KV dimensionality compression, raising three challenges:

- 1) Eliminating compression time?
- 2) Eliminating decompression time?
- 3) Eliminating the time to compute matrix R ?

To address challenge 1), given that attention computation entails matrix multiplications, a feasible strategy involves embedding the rotation matrix R into model parameters (§4.1). Consequently, the compressed matrix can be derived directly from input-parameter multiplication. Subsequently, when the compressed matrix data is multiplied with other compressed matrix data, we can simultaneously obtain the product of un-compressed matrix data, which addresses challenge 2) (§4.2). To address challenge 3), we design an offline approach to computing the compression matrix R (§4.3). Further details are elucidated in the ensuing subsections.

4.1 Eliminating Compression Time

We illustrate this rationale using K as an example for both K and V . Typically, compression is directly applied to the data to be compressed, as depicted in Fig. 7(a). After $K \in \mathbb{R}^{s \times d_h}$ is output via $K = EW_K$ (①) and utilized for computation, K is compressed by $K' = KR_p$ (②), where $K' \in \mathbb{R}^{s \times (1-p)d_h}$. Operation KR_p incurs compression overhead. KV compression happens after self-attention, and decompression happens

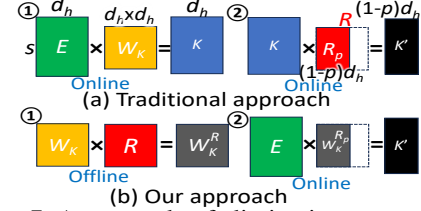


Figure 7: An example of eliminating compression.

when KV data is fetched from KVC before self-attention (as shown in the bottom of Fig. 1). This method cannot save self-attention computation time.

To eliminate compression time overhead, we design a novel method by leveraging the inherent associativity in matrix multiplication. We could pre-multiply W_K with R_p offline to have $W_K^{R_p} = W_K R_p$ so that $K' = KR_p = EW_K R_p = EW_K^{R_p}$. However, in our design, we aim to dynamically determine p value to maximize compression while satisfying an accuracy constraint (details are in §5.2). Therefore, R_p has to be determined online. To address this challenge, as shown in Fig. 7(b), we perform $W_K^R = W_K R$ offline as the new parameter matrix (①), and then drop the right p fraction of columns of W_K^R to get $W_K^{R_p}$ when generating K online (②). We will explain how to find R offline in §4.3. As shown in Fig. 8, operation $EW_K^{R_p}$ is in the QKV generation layer (① in Fig. 1) and the result K' becomes the input to self-attention (② in Fig. 1). Consequently, this operation completes the model operation and compression simultaneously. Since our method drops the p fraction of columns of W_K^R , it reduces the generation time for K .

Lemma 1 *Leveraging the associativity of matrix multiplication can eliminate the compression time overhead with a pre-determined compression matrix R .*

4.2 Eliminating Decompression Time

Using the method from §4.1, although KV can be directly compressed during QKV generation, compressed KV vectors, including those retrieved from KVC in decode, must be multiplied by R^T to decompress them before entering the subsequent self-attention layer, which incurs additional overhead, as shown in Fig. 6. To address the challenge of eliminating the decompression time, we explore whether self-attention can be performed directly on the compressed data, eliminating the need for decompression. Since the core computation of self-attention is matrix multiplication, we consider a matrix multiplication $AB^T = C$. We know that each element of C is obtained by the dot product of a row vector from A and a row vector from B . Importantly, as long as the angle between two vectors and their magnitudes remain unchanged, their dot product is invariant to rotations in space. Thus, if we rotate all row vectors of A using R , obtaining $A^R = AR$, and similarly rotate all row vectors of B to get $B^R = BR$, the equation $A^R(B^R)^T = AB^T$ will always be true.

As shown in Eq. (2), self-attention requires calculating QK^T . If we have an R that rotates Q and K to $Q^R = QR$ and $K^R = KR$, we have $Q^R(K^R)^T = QK^T$. If Q^R and K^R

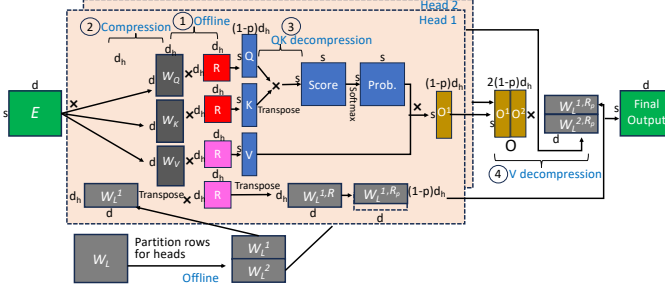


Figure 8: Illustration of ZACK’s zero-overhead compression.

have low-magnitude components in the rightmost dimensions (i.e., columns), then Q' and K' are generated by removing those dimensions from Q^R and K^R , resulting in $Q'(K')^T \approx Q^R(K^R)^T = QK^T$. Therefore, by directly calculating $Q'(K')^T$, the calculation of QK^T and the decompression operation are concurrently conducted. The compression of Q can also be integrated into QKV generation as described in §4.1. Computing $Q'(K')^T$ can reduce computation time.

Recall that given the self-attention output matrix $[P^1V^1, \dots, P^{N_h}V^{N_h}]$, the output of post-self-attention linear is calculated by $[P^1V^1, \dots, P^{N_h}V^{N_h}]W_L$ (Eq. (2) and (4)). Therefore, as for the decompression on V , we novelly pair up V and W_L and perform the decompression for V and W_L at this stage to mask the decompression latency. Then, the condition is that the V and W_L must share the same R for compression.

As shown in Fig. 8, W_L undergoes offline processing to obtain new parameters for online model operation. We evenly partition the rows of W_L to W_L^h for each head h and multiply W_L^h by the R of that head to obtain $W_L^{h,R}$. Once the compressed self-attention output $[O^1, O^2, \dots, O^{N_h}]$ is ready, we discard the bottom $p \times d_h$ rows of each $W_L^{h,R}$ and concatenate the resulting matrices vertically. Finally, we multiply the compressed self-attention output $[O^1, O^2, \dots, O^{N_h}]$ with this concatenation to yield the real output O_L (based on Eq. (4)), which reduces the computation time.

Lemma 2 *We can directly multiply compressed matrices without introducing decompression overhead to obtain the original product of uncompressed matrices if we can find a common rotation matrix R for them, by which the rotated vectors have many dimensions with low-magnitude components.*

4.3 Eliminate Compression Matrix Computation Time and Suitability of SVD

To eliminate the compression time by pairing Q - K and pairing V - W_L , a shared R is required for the paired two matrices.

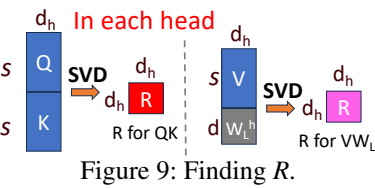


Figure 9: Finding R .

The method, as shown in Fig. 9, involves concatenating Q and K along the sequence dimension within each head and then performing SVD to obtain R . Similarly, for V - W_L , V ’s sequence dimension is concatenated with W_L^h ’s dimension of

size d (not the sliced dimension of size d_h) for SVD decomposition to derive R . However, this raises a question: does the R derived from pairing Q - K or V - W_L still ensure that the rotated vectors have many low-magnitude dimensions (as those in Fig. 5)? The answer is yes, based on the following analysis.

We calculated the average singular values for the Q - K pair and the V - W_L pair using the same method as for Fig. 5. Fig. 10 presents the results for each model and dataset. We see that, for both Q - K and V - W_L , the average singular values in the leftmost dimensions are significantly higher than those in other dimensions, indicating that Q - K and V - W_L both share many common dimensions with low-magnitude components. Consequently, the R obtained from the SVD decomposition of Q - K or V - W_L can be shared between Q and K , or between V and W_L , to eliminate the decompression overhead.

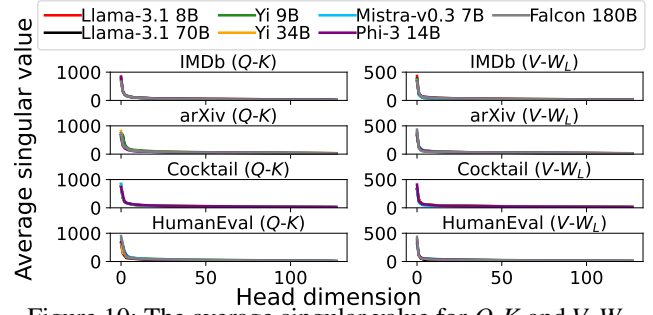


Figure 10: The average singular value for Q - K and V - W_L .

Finding common R offline. Fig. 10 has confirmed that the condition in Lemma 2 can be satisfied. However, R is still computed online. To satisfy the condition in Lemma 1—finding a pre-determined R to eliminate compression time while avoiding the overhead of computing R online—we must develop a method to obtain R that satisfies the condition of Lemma 2 offline. A key question is whether the R derived from an offline dataset can be applied to other data during inference. To answer this question, let us revisit the example in Fig. 2. In Fig. 2, for any vector in space, its transformed vector through Step ① always lies on the line $y = x$, with its component in the $y = -x$ direction guaranteed to be zero. Similarly, in QKV generation, for any token embedding vector, its transformed QKV vectors through W_Q , W_K , and W_V will certainly have low-magnitude components in certain directions. This indicates that the directions with low-magnitude components are determined by the model parameters rather than by the token embeddings. In other words, these directions are independent of datasets, implying that the Q , K , or V vectors of different datasets share common directions with low-magnitude components. Therefore, the R derived from an offline dataset can be applied to other data during inference as long as the offline dataset has sufficient tokens to capture those shared directions with low-magnitude components.

To validate this conclusion, we aim to determine whether the R derived from synthetic data, even when generated by ChatGPT, matches those obtained from real datasets. We construct a synthetic dataset by asking ChatGPT-4o [50] to gener-

ate a series of linguistically coherent articles at random. These articles have token counts ranging from 400 to 2K, with an average length of 1.4K tokens and a total token count of 57K. We compare the R derived from this synthetic dataset with the R derived from IMDb, arXiv, Cocktail, and HumanEval for each model.

Given a model, we use the constructed dataset to collect all QKV vectors and derive the rotation matrix $\bar{R}_{QK}^{h,l}$ for Q - K and $\bar{R}_{VW}^{h,l}$ for V - W_L in head h of layer l as described in Fig. 9. Similarly, for a dataset a , we apply the same method to obtain its corresponding $R_{QK}^{a,h,l}$ and $R_{VW}^{a,h,l}$. We use AABS(M) to denote the average absolute value of all elements in matrix M and $\text{SUB}(M_1, M_2)$ to denote the element-wise subtraction of M_2 from M_1 . For a model and a dataset a , taking Q - K as an example, we compute $\bar{\epsilon} = \frac{1}{N_h N_l} \sum_{h=1}^{N_h} \sum_{l=1}^{N_l} \text{AABS}(\bar{R}_{QK}^{a,h,l})$ to evaluate the average magnitude of an individual element in $R_{QK}^{a,h,l}$. We also calculate $\bar{\delta} = \frac{1}{N_h N_l} \sum_{h=1}^{N_h} \sum_{l=1}^{N_l} \text{AABS}(\text{SUB}(\bar{R}_{QK}^{h,l}, R_{QK}^{a,h,l}))$ to evaluate the average magnitude of the differences between the elements of $\bar{R}_{QK}^{h,l}$ and $R_{QK}^{a,h,l}$. Similarly, we calculate $\bar{\epsilon}$ and $\bar{\delta}$ for the V - W_L pair as well.

$\langle \bar{\epsilon}, \bar{\delta} \rangle$	IMDb	arXiv	Cocktail	HumanEval
Llama-3.1 8B	$\langle 5.29e-2, 1.1e-4 \rangle$	$\langle 5.27e-2, 1.5e-4 \rangle$	$\langle 5.28e-2, 8e-5 \rangle$	$\langle 5.3e-2, 1.7e-4 \rangle$
Llama-3.1 70B	$\langle 5.54e-2, 9.5e-5 \rangle$	$\langle 5.53e-2, 1.3e-4 \rangle$	$\langle 5.54e-2, 8.4e-5 \rangle$	$\langle 5.52e-2, 1.6e-4 \rangle$
Yi 9B	$\langle 5.05e-2, 1.7e-4 \rangle$	$\langle 5.08e-2, 4.9e-5 \rangle$	$\langle 5.06e-2, 7.6e-5 \rangle$	$\langle 5.06e-2, 1.2e-4 \rangle$
Yi 34B	$\langle 5.92e-2, 1.4e-4 \rangle$	$\langle 5.93e-2, 5.1e-5 \rangle$	$\langle 5.94e-2, 3.9e-5 \rangle$	$\langle 5.92e-2, 1.7e-4 \rangle$
Mistral-v0.3 7B	$\langle 6.43e-2, 8.3e-5 \rangle$	$\langle 6.41e-2, 1.8e-4 \rangle$	$\langle 6.44e-2, 7.1e-5 \rangle$	$\langle 6.43e-2, 4.5e-5 \rangle$
Phi-3 14B	$\langle 5.41e-2, 1.9e-4 \rangle$	$\langle 5.43e-2, 5.2e-5 \rangle$	$\langle 5.44e-2, 1.1e-4 \rangle$	$\langle 5.44e-2, 4.6e-5 \rangle$
Falcon 180B	$\langle 6.22e-2, 8.7e-5 \rangle$	$\langle 6.22e-2, 1.3e-4 \rangle$	N/A	$\langle 6.25e-2, 1.5e-4 \rangle$

Table 4: $\bar{\epsilon}$ and $\bar{\delta}$ for the Q - K pair.

$\langle \bar{\epsilon}, \bar{\delta} \rangle$	IMDb	arXiv	Cocktail	HumanEval
Llama-3.1 8B	$\langle 6.77e-2, 4.6e-5 \rangle$	$\langle 6.78e-2, 3.1e-5 \rangle$	$\langle 6.78e-2, 5.3e-5 \rangle$	$\langle 6.76e-2, 9.4e-5 \rangle$
Llama-3.1 70B	$\langle 6.13e-2, 8.1e-5 \rangle$	$\langle 6.15e-2, 9.6e-5 \rangle$	$\langle 6.15e-2, 6.2e-5 \rangle$	$\langle 6.13e-2, 7.8e-5 \rangle$
Yi 9B	$\langle 5.59e-2, 9.3e-5 \rangle$	$\langle 5.62e-2, 1.4e-4 \rangle$	$\langle 5.61e-2, 4.9e-5 \rangle$	$\langle 5.61e-2, 7.4e-5 \rangle$
Yi 34B	$\langle 6.64e-2, 1e-4 \rangle$	$\langle 6.64e-2, 8.8e-5 \rangle$	$\langle 6.66e-2, 3.5e-5 \rangle$	$\langle 6.65e-2, 5.1e-5 \rangle$
Mistral-v0.3 7B	$\langle 7.04e-2, 9.2e-5 \rangle$	$\langle 7.06e-2, 1.1e-4 \rangle$	$\langle 7.06e-2, 5.7e-5 \rangle$	$\langle 7.05e-2, 3.4e-5 \rangle$
Phi-3 14B	$\langle 6.32e-2, 5.5e-5 \rangle$	$\langle 6.32e-2, 7.5e-5 \rangle$	$\langle 6.33e-2, 4.4e-5 \rangle$	$\langle 6.32e-2, 9.3e-5 \rangle$
Falcon 180B	$\langle 7.27e-2, 1.3e-4 \rangle$	$\langle 7.27e-2, 1.5e-4 \rangle$	N/A	$\langle 7.29e-2, 6.4e-5 \rangle$

Table 5: $\bar{\epsilon}$ and $\bar{\delta}$ for the V - W_L pair.

Table 4 and Table 5 present $\bar{\epsilon}$ and $\bar{\delta}$ for Q - K and V - W_L , respectively, displayed in the format $\langle \bar{\epsilon}, \bar{\delta} \rangle$. We observe that the average variation $\bar{\delta}$ in the values of individual elements of R is less than 0.34% of the average absolute value $\bar{\epsilon}$ of a single element. This upper limit is derived from the results in Table 4 for Yi 9B with IMDb. This indicates that the R derived from the synthetic dataset is highly similar to the R derived from a different dataset, with minimal variation. In other words, the R computed offline even using the synthetic dataset can be applied to other datasets to compress QKV. This validates the earlier conclusion and satisfies the conditions of Lemma 1 and Lemma 2. §6.6 illustrates the impact of different numbers of tokens in the synthetic dataset on the offline-computed R .

Lemma 3 *When using a dataset with a sufficient number of tokens constructed from linguistically coherent sentences,*

we can compute R offline using SVD, which satisfies the conditions of Lemmas 1 and 2 for designing the zero-overhead compression method.

5 Design of ZACK

5.1 SVD-based Zero-Overhead Compression

Fig. 8 demonstrates the workflow of how ZACK performs the zero-overhead compression. It consists of 1) Offline rotation matrix computation (§5.1), 2) QK compression and decompression (§5.1), and 3) VW_L compression and decompression (§5.1), as explained in the following sections.

Offline rotation matrix computation. Computing R for Q - K and V - W_L using a synthetic dataset offline (① in Fig. 8) is explained in §4.3.

QK compression and decompression. We perform $W_Q^{R,h} = W_Q^h R^h$ and $W_K^{R,h} = W_K^h R^h$ offline. We determine the compression rate p online (details are in §5.2). During inference, Eq. (1) is executed (②), where we simply remove the right p fraction of the columns of $W_Q^{R,h}$ and $W_K^{R,h}$. Consequently, the output of the QK generation layer will be the compressed Q and K . Subsequently, self-attention computes QK^T using the compressed Q and K in Eq. (2). This process approximates the original QK^T based on Lemma 2 without necessitating specific decompression operations (③).

VW_L compression and decompression. V is compressed in the same manner as Q and K . That is, we perform $W_V^h = W_V^h R_h$ offline. Pairing V with W_L helps eliminate the decompression time of V . In contrast to online QKV generation, W_L undergoes offline processing to obtain new parameters for online model operation. That is, the linear layer parameter matrix $[W_L^1, \dots, W_L^{N_h}]$ is updated by $[W_L^1 R^1, \dots, W_L^{N_h} R^{N_h}]$. During inference, once the compressed self-attention output O is prepared, we simply discard $p \times d_h$ dimensions from each $W_L^{R,h}$ and concatenate them together. This concatenated matrix is then multiplied with O to obtain the output O_L (④ in Fig. 8).

Rotary embedding. Fig. 8 presents ZACK atop a standard transformer model. However, recent models such as Llama-3.1 and Yi employ Rotary Position Embedding (RoPE) [51], which processes temporarily generated $Q_{tmp} = EW_Q$ and $K_{tmp} = EW_K$ to obtain Q and K to be used in self-attention. Specifically, RoPE rotates each row vector q and k of Q_{tmp} and K_{tmp} using a rotation matrix H_i , where i is the position of q and k in the sequence. The existence of RoPE prevents the integration of R of Q - K into W_Q and W_K to eliminate QK compression time. As shown in Fig. 6, the overhead of compression is relatively small compared to that of decompression because compression is performed once per token, whereas decompression is performed every decode iteration. Therefore, for RoPE-based models, we compress Q and K using R online and do not integrate R into W_Q and W_K . However, for the V - W_L pair, we still integrate their R into W_V and W_L .

5.2 Adaptive Compression Rate Determination

Model layers contribute differently to the output [16], as do the attention heads within each layer [18]. This implies that the distribution of singular values obtained through SVD for $Q\text{-}K$ and $V\text{-}W_L$ may vary across different heads and layers. Table 6 and 7 present the coefficient of variation (CV) of the maximum singular values (i.e., those in the first head dimension) for $Q\text{-}K$ and $V\text{-}W_L$, respectively, across all heads of each model with different datasets. The CV is the ratio of the standard deviation to the mean of the maximum singular values of heads. This CV for different models and datasets is around 40%-50%, indicating significant variation in the maximum singular values among different heads.

	IMDb	arXiv	Cocktail	HumanEval
Llama-3.1 8B	51.13%	51.21%	51.07%	50.94%
Llama-3.1 70B	57.75%	58.03%	57.69%	57.51%
Yi 9B	48.44%	48.17%	48.72%	48.51%
Yi 34B	55.21%	55.73%	54.95%	54.98%
Mistral-v0.3 7B	49.76%	49.55%	49.93%	50.04%
Phi-3 14B	52.97%	53.38%	52.63%	52.53%
Falcon 180B	53.76%	53.25%	N/A	53.41%

Table 6: CV of the maximum singular values for $Q\text{-}K$.

	IMDb	arXiv	Cocktail	HumanEval
Llama-3.1 8B	43.59%	43.63%	43.56%	43.61%
Llama-3.1 70B	45.16%	45.42%	45.38%	44.95%
Yi 9B	41.39%	40.77%	41.02%	41.54%
Yi 34B	44.48%	44.81%	44.96%	44.52%
Mistral-v0.3 7B	41.86%	42.37%	41.44%	41.31%
Phi-3 14B	45.37%	44.82%	44.96%	45.69%
Falcon 180B	42.58%	42.79%	N/A	42.83%

Table 7: CV of the maximum singular values for $V\text{-}W_L$.

Since the dominant maximum singular values vary across heads, the compression rate p for each head should also differ. For heads with larger maximum singular values and more dimensions with relatively smaller values, we can use a higher p to remove more low-magnitude dimensions. Conversely, for heads with smaller maximum singular values and fewer dimensions with relatively smaller values, we can use a lower p to remove fewer low-magnitude dimensions. This can achieve a higher overall compression rate p with minimal accuracy loss. How to determine p for $Q\text{-}K$ and $V\text{-}W_L$ in each head remains a question. Since singular values represent the magnitude of the components of rotated vectors in their corresponding dimensions, the proportion of the cumulative sum of the removed singular values to the total sum of singular values determines the extent of information loss. We introduce a singular value removal rate r to control this proportion, which is the ratio of the sum of the singular values in the removed dimensions to the total sum of the singular values across all d_h dimensions. In a head, given an r , the corresponding p for $Q\text{-}K$ or $V\text{-}W_L$ can be determined. Specifically, given an r , we only need to find p that satisfies the following condition:

$$\frac{\sum_{i=j+1}^{d_h-1} s^i}{\sum_{i=0}^{d_h-1} s^i} \leq r < \frac{\sum_{i=j}^{d_h-1} s^i}{\sum_{i=0}^{d_h-1} s^i} \text{ AND } j = \lfloor (1-p)(d_h - 1) \rfloor, \quad (6)$$

where s^i is the singular value at head dimension i . We set a shared r for all heads across different layers, allowing us to directly determine the p required for $Q\text{-}K$ and $V\text{-}W_L$ in each head, thereby obtaining the overall KV compression rate. This enables us to construct a function F_p that takes the overall KV compression rate as input and outputs the combination of p needed for all heads. During inference, based on the overall compression rate required for KV, we use F_p to directly obtain the p needed for $Q\text{-}K$ and $V\text{-}W_L$ in each head.

5.3 Kernel Enhancement for Adaptive Compression Rate

State-of-the-art memory-efficient self-attention kernel implementations (e.g., FlashAttention-2 [52]) operate as shown in Fig. 11. The self-attention computation of a batch of requests is divided into $batch_size \times N_h$ computation units, each corresponding to a head of a request. Each unit further splits Q into blocks of shape $(B_r = 64, d_{qk} = d_h)$, where B_r is the row block size and d_{qk} is the head dimension size for Q and K . Each Q block is processed on one SM as an SM task. All SMs responsible for a head share that head's K and V to minimize data movement between SMs, thereby reducing memory access overhead. When an SM processes a Q block, K , and V , it further divides K and V into blocks of shape $(B_c = 64, d_v = d_h)$ to be processed sequentially in time order, where B_c is the column block size and d_v is the head dimension size for V . Without adaptive compression rates, all heads use the same d_{qk} and the same d_v . However, with adaptive compression rates, different heads have different d_{qk} and different d_v , resulting in varying computational loads and uneven execution times for each SM. The kernel runtime is determined by the SM with the longest execution time. Therefore, it is necessary to enhance the self-attention kernel with adaptive compression rates. We propose different enhancements for prefill and decode.

Prefill. During prefill, the computational workload of an SM task includes $2B_r d_{qk} s_{kv}$ for multiplying the Q block with K , $2B_r s_{kv}$ for softmax, and $2B_r s_{kv} d_v$ for multiplying attention probability with V , resulting in a total of $2B_r s_{kv} (d_{qk} + d_v + 1)$, where s_{kv} is the sequence length of K and V . Let $d_{sum}^i = d_{qk} + d_v + 1$ for head i and d_{sum}^{max} be the maximum d_{sum}^i across all heads. As the compression rate changes, d_{sum}^i changes accordingly. We increase B_r to $\frac{d_{sum}^{max}}{d_{sum}^i} B_r$ for head i , ensuring that the computational workload for each SM task is the same,

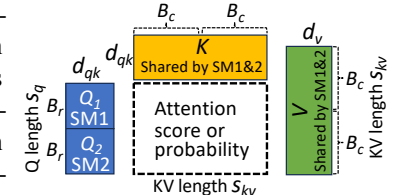


Figure 11: Self-attention kernel. is divided into $batch_size \times N_h$ computation units, each corresponding to a head of a request. Each unit further splits Q into blocks of shape $(B_r = 64, d_{qk} = d_h)$, where B_r is the row block size and d_{qk} is the head dimension size for Q and K . Each Q block is processed on one SM as an SM task. All SMs responsible for a head share that head's K and V to minimize data movement between SMs, thereby reducing memory access overhead. When an SM processes a Q block, K , and V , it further divides K and V into blocks of shape $(B_c = 64, d_v = d_h)$ to be processed sequentially in time order, where B_c is the column block size and d_v is the head dimension size for V . Without adaptive compression rates, all heads use the same d_{qk} and the same d_v . However, with adaptive compression rates, different heads have different d_{qk} and different d_v , resulting in varying computational loads and uneven execution times for each SM. The kernel runtime is determined by the SM with the longest execution time. Therefore, it is necessary to enhance the self-attention kernel with adaptive compression rates. We propose different enhancements for prefill and decode.

preventing uneven execution times among SMs. By increasing B_r , the number of Q blocks per head decreases, reducing the total number of SM tasks. As a result, the GPU can complete all SM tasks in fewer rounds, with each round using all SMs of the GPU. In the final round, not all SMs may be fully utilized. To maximize the utilization, we redistribute the remaining SM tasks in the last round. Suppose the GPU has N_{SM} SMs and the last round has N_{last} SM tasks. The workload assigned to each SM should be $wl = \frac{1}{N_{SM}} \sum_{i=1}^{N_{last}} B_r^{tsk(i)} d_{sum}^{tsk(i)}$, where $B_r^{tsk(i)}$ and $d_{sum}^{tsk(i)}$ is B_r and d_{sum} of the i -th SM task in the last round. Then, task i should be split into smaller blocks using new row block size $wl/d_{sum}^{tsk(i)}$. All redistributed tasks in the last round are sequentially assigned to an SM with the smallest allocated workloads one at a time.

Decode. In decode, the Q length s_q for each head is only 1, meaning it cannot be divided into multiple Q blocks. Consequently, each head corresponds to one SM task, and adjusting B_r to enhance the kernel is not feasible. Instead, we schedule these tasks in a heuristic way to avoid heavy overhead. The execution time of each task k_i is determined by $s_{kv} \times d_{sum}$. All tasks are sorted in descending order of execution time and then sequentially assigned to an SM with the smallest cumulative assigned time one at a time. Fig. 12 provides an example where 7 tasks are distributed across 3 SMs. Tasks k_1 - k_7 are sorted in descending order of execution time. Following our scheduling strategy, k_1 and k_6 are assigned to SM1, k_2 , k_5 , and k_8 to SM2, and k_3 , k_4 , and k_7 to SM3.

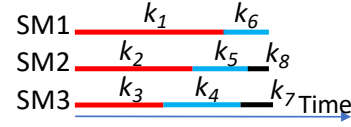


Figure 12: Task allocation.

6 Performance Evaluation

6.1 Implementation

We implemented ZACK based on vLLM [48] and modified vLLM model classes to enable QKV compression and adaptive compression rates. We used NVIDIA CUTLASS [53] to implement the on-device matrix multiplication for the self-attention kernel. A load balancer was implemented with a fast Python web framework Quart [54], which allocates each request to a vLLM instance with the shortest queue length.

Kernel enhancement for prefill. For prefill-stage kernel enhancement (§5.3), a large B_r can cause data to exceed the register capacity of a single SM. In such cases, we reduce B_r to prevent this issue, which does not affect the total computational workload of an SM task since s_{kv} remains unchanged. Limited by the tensor core interface used for matrix operations, the values of d_{qk} , d_v , B_r , and B_c must be multiples of 16. Therefore, these values are rounded up to the nearest multiple of 16, and any padding required is filled with zeros. For a given overall KV compression rate p , the d_{sum} and B_c for each head are determined, and B_r used by each head is also determined except in the final round. In the last round, B_r can be enumerated among multiples of 16. For different over-

all KV compression rates, we pre-compile all kernels offline according to the required matrix shapes.

Kernel enhancement for decode. For decode-stage kernel enhancement, we fused the scheduling computations (a significant portion of which involves sorting) to a CUDA kernel, thereby minimizing the time overhead.

6.2 Compared Methods

ZACK is the first zero-overhead KV dimensionality compression method, and it can complement token eviction-based and quantization-based methods. We selected the most representative state-of-the-art eviction-based method, Keyformer [22], and the quantization-based method, KVQuant [31], as comparison methods. We combined ZACK with Keyformer and KVQuant to create enhanced versions, referred to as Keyformer-Z and KVQuant-Z, respectively. The baseline method does not have KV compression.

Keyformer-Z. It uses ZACK to obtain compressed KV and then applies Keyformer to evict KV. Self-attention is performed with ZACK’s decompression-free method.

KVQuant-Z. The basic way involves first using ZACK to compress KV, followed by applying KVQuant to quantize the compressed KV. During decompression, they are first dequantized and then processed with ZACK’s decompression-free method. For RoPE-based models, since KVQuant compresses K before RoPE by default, while ZACK compresses K after RoPE, we configure both ZACK and KVQuant to compress K after RoPE, enabling KVQuant-Z to function in the previously described basic way for RoPE-based models.

	Baseline	ZACK	Keyformer	Keyformer-Z	KVQuant	KVQuant-Z
	Accuracy	Overall compression rate for 99% of baseline accuracy				
Llama-3.1 8B	91.67%	0.53	0.43	0.72	0.75	0.89
Llama-3.1 70B	95.73%	0.63	0.46	0.74	0.75	0.91
Yi 9B	85.29%	0.59	0.39	0.68	0.75	0.88
Yi 34B	93.98%	0.55	0.44	0.75	0.75	0.92
Mistral-v0.3 7B	84.81%	0.61	0.40	0.71	0.75	0.90
Phi-3 14B	87.85%	0.58	0.45	0.80	0.75	0.92
Falcon 180B	85.53%	0.49	0.41	0.73	0.75	0.87

Table 8: KV compression rate (IMDb).

	Baseline	ZACK	Keyformer	Keyformer-Z	KVQuant	KVQuant-Z
	Accuracy	Overall compression rate for 99% of baseline accuracy				
Llama-3.1 8B	81.57%	0.65	0.58	0.84	0.75	0.90
Llama-3.1 70B	83.85%	0.67	0.63	0.86	0.75	0.92
Yi 9B	82.42%	0.57	0.63	0.85	0.75	0.92
Yi 34B	87.73%	0.64	0.69	0.87	0.75	0.91
Mistral-v0.3 7B	79.40%	0.64	0.61	0.84	0.75	0.92
Phi-3 14B	86.36%	0.62	0.59	0.82	0.75	0.91
Falcon 180B	79.94%	0.60	0.63	0.85	0.75	0.90

Table 9: KV compression rate (arXiv).

	Baseline	ZACK	Keyformer	Keyformer-Z	KVQuant	KVQuant-Z
	Accuracy	Overall compression rate for 99% of baseline accuracy				
Llama-3.1 8B	76.24%	0.56	0.51	0.75	0.75	0.91
Llama-3.1 70B	86.39%	0.59	0.65	0.84	0.75	0.92
Yi 9B	77.16%	0.52	0.54	0.77	0.75	0.89
Yi 34B	85.25%	0.60	0.62	0.83	0.75	0.92
Mistral-v0.3 7B	75.18%	0.58	0.57	0.79	0.75	0.90
Phi-3 14B	83.92%	0.69	0.61	0.82	0.75	0.92

Table 10: KV compression rate (Cocktail).

	Baseline	ZACK	Keyformer	Keyformer-Z	KVQuant	KVQuant-Z
Accuracy	Overall compression rate for 99% of baseline accuracy					
Llama-3.1 8B	87.53%	0.54	0.46	0.76	0.75	0.87
Llama-3.1 70B	94.45%	0.56	0.51	0.77	0.75	0.87
Yi 9B	85.82%	0.55	0.48	0.72	0.75	0.86
Yi 34B	90.79%	0.59	0.53	0.78	0.75	0.90
Mistral-v0.3 7B	89.37%	0.53	0.50	0.73	0.75	0.89
Phi-3 14B	91.62%	0.54	0.58	0.77	0.75	0.91
Falcon 180B	85.21%	0.58	0.47	0.74	0.75	0.92

Table 11: KV compression rate (HumanEval).

6.3 Accuracy Performance

We study the relationship between accuracy and the overall KV compression rate p . Specifically, we focus on the scenarios where the methods achieve 99% of the baseline accuracy [22]. For Keyformer-Z, we configure the ZACK and Keyformer components to contribute equally to the overall compression rate. Since KVQuant can only be configured with 2-4 quantization bit widths, we use 4-bit quantization for both KVQuant and KVQuant-Z to ensure the accuracy reaches 99% of the baseline. We use binary search to determine the maximum p that achieves 99% of the baseline accuracy. Table 8-11 show the results for different datasets. ZACK alone achieves p of 0.49-0.69 across all datasets. Keyformer and KVQuant achieve p of 0.39-0.64 and 0.75, respectively. Keyformer-Z and KVQuant-Z achieve p of 0.68-0.83 and 0.87-0.92, further reducing the size of KV by 45.24%-63.61% and 48%-68% compared to Keyformer and KVQuant, respectively. The improvement stems from dimensionality compression with the adaptive compression rate.

6.4 Overall System Performance

We used the same server setting as in §3 unless otherwise specified. We tested Mistral-v0.3 7B, Phi-3 14B, Yi 34B, Llama-3.1 70B, and Falcon 180B, denoted by M, P, Y, L, and F. The KV compression rates for them follow those in Table 8-11.

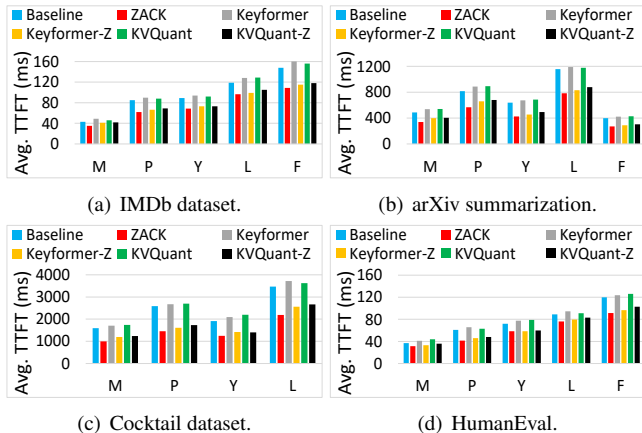


Figure 13: Average TTFT under different datasets.

Fig. 13 shows the average TTFT over requests for different models and datasets. For IMDb, arXiv, Cocktail, and HumanEval, ZACK reduces TTFT by 17%-33%, 34%-42%, 37%-48%, and 18%-29%, respectively, compared to the baseline. This is because ZACK not only reduces the QKV generation time but also computes on compressed data during

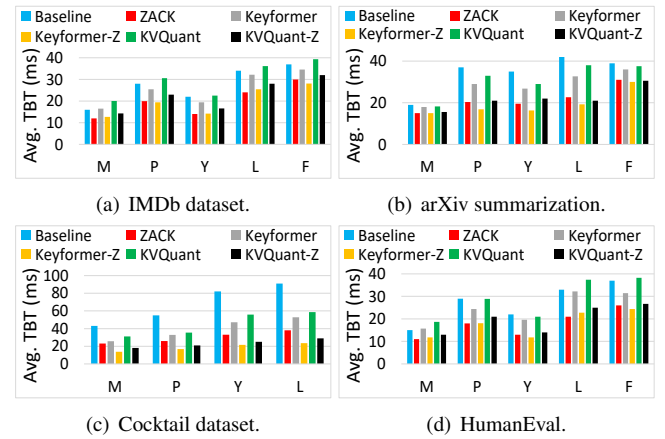


Figure 14: Average TBT under different datasets.

attention, thereby reducing latency while avoiding decompression overhead. Additionally, ZACK leverages adaptive compression rates and self-attention kernel enhancement to further reduce self-attention time. The improvement is particularly significant for arXiv and Cocktail, as these datasets have longer input lengths, meaning that attention time constitutes a higher proportion of TTFT. Consequently, the reduction in attention time contributes more to the overall TTFT reduction. For IMDb, arXiv, Cocktail, and HumanEval, Keyformer-Z improves Keyformer by 17%-30%, 31%-38%, 34%-44%, and 17%-26%, respectively. KVQuant-Z improves KVQuant by 15%-25%, 24%-31%, 29%-38%, and 18%-24%, respectively. These improvements arise from the benefits provided by ZACK, as described before.

Fig. 14 shows the average TBT over requests for different models and datasets. For IMDb, arXiv, Cocktail, and HumanEval, ZACK reduces TBT by 23%-47%, 25%-54%, 57%-61%, and 25%-45%, respectively, compared to the baseline. In addition to the reasons mentioned above, the improvement in TBT also stems from the reduced memory overhead due to the smaller KV size. For these datasets, Keyformer-Z improves Keyformer by 20%-37%, 22%-49%, 51%-55%, and 24%-38%, respectively. KVQuant-Z improves KVQuant by 18%-28%, 18%-44%, 40%-53%, and 27%-33%, respectively. Keyformer-Z and KVQuant-Z benefit from ZACK for the same reasons outlined before.

We vary the overall request rate, Request Per Second (RPS), and record the normalized latency for each output token [48], calculated by dividing the end-to-end time (i.e., JCT) by the number of output tokens. Fig. 15 shows the normalized latency versus RPS for all models and datasets. When the RPS exceeds capacity, the queue length grows faster than the processing speed, leading to an infinite increase in queuing time and latency. Compared to the baseline, ZACK achieves 1.69-2.17 \times , 1.59-2.08 \times , 1.52-1.98 \times , and 1.65-2.24 \times RPS for IMDb, arXiv, Cocktail, and HumanEval, respectively, while preserving the same latency; Keyformer achieves 1.37-1.59 \times , 1.49-2.02 \times , 1.44-1.97 \times , and 1.46-2.1 \times RPS; KVQuant achieves 1.77-2.49 \times , 1.68-2.64 \times ,

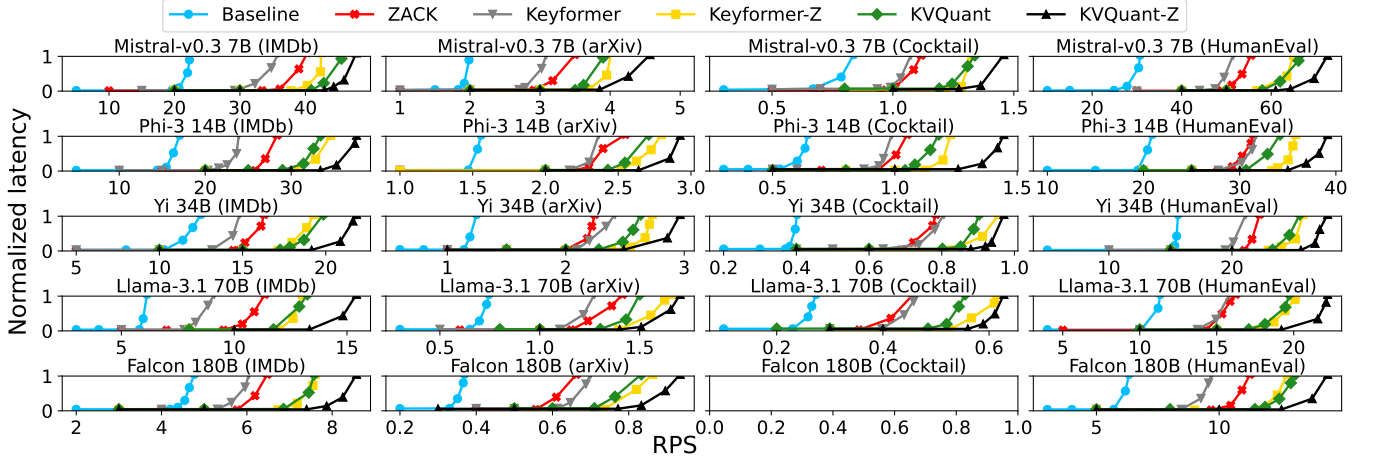


Figure 15: Normalized latency under different RPS.

1.95-2.53 \times , and 1.67-2.58 \times RPS. The higher the KV compression rate, the higher the maximum RPS that can maintain a constant low latency. Regarding this maximum RPS, Keyformer-Z achieves 1.3-1.63 \times , 1.27-1.59 \times , 1.31-1.72 \times , and 1.26-1.48 \times RPS compared to Keyformer; KVQuant-Z achieves 1.15-1.24 \times , 1.14-1.22 \times , 1.13-1.32 \times , and 1.12-1.23 \times RPS compared to KVQuant. ZACK further improves Keyformer and KVQuant because it further reduces the size of KV to enable larger batch sizes.

6.5 Ablation Study

We test the variants of ZACK as follows to evaluate each individual method. 1) ZACK/OE is ZACK without compression/decompression Overhead Elimination. It computes R and performs compression and decompression for KV online, conducting self-attention on uncompressed data. 2) ZACK/AC is ZACK without Adaptive Compression rate. It uses the same compression rate for all heads to achieve 99% of baseline accuracy. 3) ZACK/KE is ZACK without self-attention Kernel Enhancement.

Fig. 16 and Fig. 17 show the average TTFT and TBT over requests for individual methods with different models and datasets. As shown in Fig. 16, ZACK/OE has 75%-121%, 82%-164%, 89%-178%, and 91%-136% higher TTFT than ZACK for IMDb, arXiv, Cocktail, and HumanEval because ZACK/OE computes R online, uses uncompressed data for computation, and performs online compression of KV. ZACK/AC has 20%-29%, 21%-32%, 24%-33%, and 17%-44% higher TTFT than ZACK because, without the adaptive compression rate, the overall KV compression rate required to achieve 99% of the baseline accuracy is lower, thereby increasing attention time. ZACK/KE has 11%-23%, 20%-31%, 33%-38%, and 8%-22% higher TTFT than ZACK due to the uneven computation times of SMs. In Fig. 17, ZACK/OE has 64%-86%, 71%-91%, 78%-127%, and 61%-82% higher TBT than ZACK for IMDb, arXiv, Cocktail, and HumanEval. ZACK/AC has 16%-21%, 14%-59%, 23%-45%, and 11%-23% higher TBT than ZACK. ZACK/KE has 18%-36%, 19%-38%,

34%-52%, and 26%-40% higher TBT than ZACK. The reasons for the TBT degradation of ZACK/AC and ZACK/KE are the same as explained for TTFT. ZACK/OE has a higher TBT degradation compared to ZACK/AC and ZACK/KE because it decompresses KV every decode iteration.

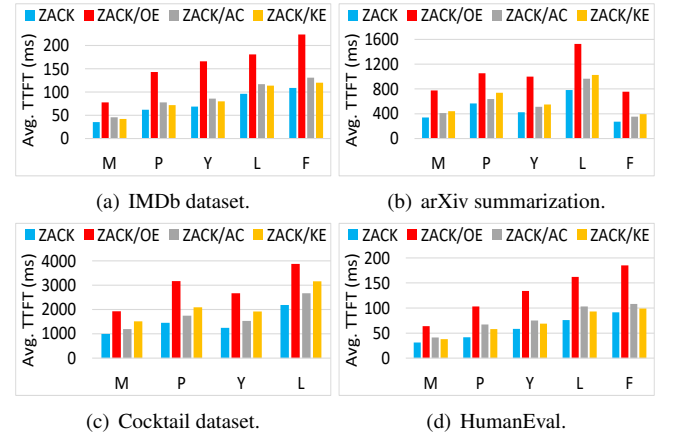


Figure 16: Average TTFT for individual methods.

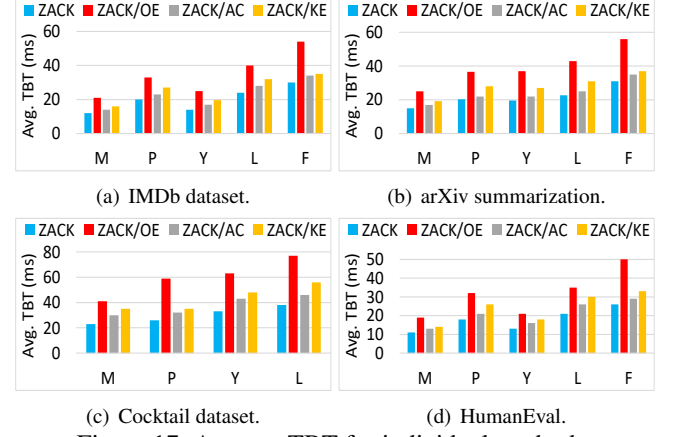


Figure 17: Average TBT for individual methods.

6.6 Sensitivity Testing

We vary the total number of tokens in the synthetic dataset used for offline computation of R to study its impact on R .

Given a synthetic dataset with a specific number of tokens, for each model’s Q - K pair or V - W_L pair, we calculate the ratio $\bar{\delta}/\bar{\epsilon}$ in §4.3 for each dataset and calculate their average across datasets. The smaller $\bar{\delta}/\bar{\epsilon}$, the more accurate R is. Fig. 18 shows this average ratio across datasets for Q - K and V - W_L of each model. The results show that when the synthetic dataset contains a sufficient number of tokens greater than 16K constructed from linguistically coherent sentences, the average ratio $\bar{\delta}/\bar{\epsilon}$ across datasets for all models is below 0.5% for both Q - K and V - W_L , ensuring the accuracy of the offline-computed R . The rationale for this has already been explained in §4.3 to support the conclusion in that section.

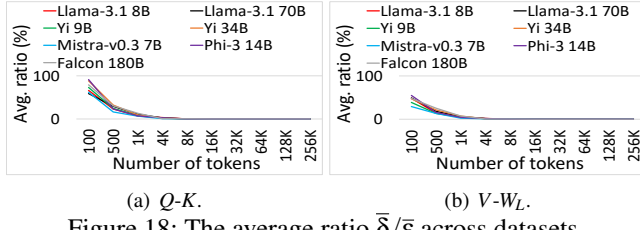


Figure 18: The average ratio $\bar{\delta}/\bar{\epsilon}$ across datasets.

6.7 Time Overhead

We study the online time overhead introduced by SM scheduling in the self-attention kernel. We record the number of GPU cycles occupied by the scheduling computation and use this to estimate scheduling time. Finally, we calculate the proportion of scheduling time relative to the end-to-end latency. Table 12 presents the 99th percentile (P99) time overhead ratio for different models and datasets. As the model size increases and the input length becomes longer, the P99 time overhead ratio tends to decrease. This is because larger models and longer sequences spend more time on computation, thereby reducing the proportion of the overhead. The P99 time overhead does not exceed 4.13% of the end-to-end latency, making the scheduling overhead acceptable.

	IMDb	arXiv	Cocktail	HumanEval
Llama-3.1 8B	3.57%	2.74%	2.37%	3.81%
Llama-3.1 70B	3.19%	2.39%	1.98%	3.75%
Yi 9B	3.82%	2.66%	2.35%	4.13%
Yi 34B	2.94%	1.85%	1.64%	3.52%
Mistral-v0.3 7B	3.46%	2.21%	1.96%	3.98%
Phi-3 14B	2.83%	2.37%	2.27%	3.54%
Falcon 180B	2.19%	1.72%	N/A	2.77%

Table 12: P99 overhead compared to end-to-end time.

7 Limitations and Future Work

RoPE. For RoPE-based models, we are currently unable to integrate the offline-computed R for Q - K into W_Q and W_K to eliminate the compression time. However, compression is a one-time operation, whereas KV decompression is repeated in every decode iteration. As shown in Fig. 6, the compression time constitutes a much smaller portion of the overall JCT compared to the decompression time. Therefore, it is acceptable not to eliminate the QK compression time for RoPE-based models. We will still address it in the future work.

Kernel enhancement. The enhancement of the self-attention kernel with adaptive compression rates relies on a simple heuristic method for workload scheduling. In the future, we will optimize this approach to minimize self-attention latency.

8 Related Work

Eviction. Many KV compression methods are based on token eviction [17–26], also known as pruning. The main idea is to remove unimportant tokens’ KV that have minimal impact on inference results. The methods in [17–24] determine token importance based on attention scores. Tokens with lower scores are considered less important, and their KV can be discarded. The methods in [25, 26] achieve sparse attention by identifying low-score regions in the attention score matrix and removing KV in those regions. Eviction-based methods reduce KV along the sequence dimension, while ZACK reduces KV along the hidden dimension.

Quantization. Many methods use quantization to compress KV [27–31]. The basic idea is to compress each element of KV by reducing high-bit representations, such as float16, to lower-bit representations, such as 4-bit or even 2-bit. It reduces the number of bits required to store KV. However, during attention computation, the quantized KV must first be dequantized to recover the original data, introducing decompression overhead. ZACK, on the other hand, reduces the total number of elements of K and V . As such, it can complement quantization methods. ZACK can first compress the dimensionality of KV to reduce the total number of elements, followed by quantization to compress the individual elements.

Low-rank approximation. Recently, some methods have attempted to use low-rank approximations to reduce the hidden size of KV [55, 56]. However, these methods still require decompressing KV during attention and cannot compute on the compressed data to reduce computation time. ZACK not only eliminates decompression overhead but also reduces attention computation time by performing computation on the compressed data.

9 Conclusion

In this paper, we introduce ZACK, the first KV dimensionality compression system that achieves zero-overhead compression and decompression and also reduces computation time. It can serve as a complementary approach to existing token eviction- and quantization-based KV compression methods. Comprehensive experiments show that compared to the baseline without compression, ZACK achieves up to a 0.69 KV compression rate, reduces TTFT by up to 48% and TBT by up to 61%, and delivers up to $2.24\times$ throughput under the same latency, while maintaining 99% of the baseline accuracy. When combined with ZACK, state-of-the-art eviction-based and quantization-based methods for KV compression further reduce KV size by up to 68%, TTFT by up to 44%, and TBT by up to 55% and achieve up to $1.72\times$ throughput under the same latency, while maintaining 99% of the baseline accuracy.

References

[1] Alec Radford, Karthik Narasimhan, Tim Salimans, Ilya Sutskever, et al. Improving language understanding by generative pre-training. 2018.

[2] Jacob Devlin, Ming-Wei Chang, Kenton Lee, and Kristina Toutanova. BERT: pre-training of deep bidirectional transformers for language understanding. *CoRR*, abs/1810.04805, 2018.

[3] Alec Radford, Jeffrey Wu, Rewon Child, David Luan, Dario Amodei, Ilya Sutskever, et al. Language models are unsupervised multitask learners. *OpenAI blog*, 1(8):9, 2019.

[4] Tom Brown, Benjamin Mann, Nick Ryder, Melanie Subbiah, Jared D Kaplan, Prafulla Dhariwal, Arvind Neelakantan, Pranav Shyam, Girish Sastry, Amanda Askell, Sandhini Agarwal, Ariel Herbert-Voss, Gretchen Krueger, Tom Henighan, Rewon Child, Aditya Ramesh, Daniel Ziegler, Jeffrey Wu, Clemens Winter, Chris Hesse, Mark Chen, Eric Sigler, Mateusz Litwin, Scott Gray, Benjamin Chess, Jack Clark, Christopher Berner, Sam McCandlish, Alec Radford, Ilya Sutskever, and Dario Amodei. Language models are few-shot learners. In H. Larochelle, M. Ranzato, R. Hadsell, M.F. Balcan, and H. Lin, editors, *Advances in Neural Information Processing Systems*, volume 33, pages 1877–1901. Curran Associates, Inc., 2020.

[5] Timo Schick, Jane Dwivedi-Yu, Roberto Densi, Roberta Raileanu, Maria Lomeli, Luke Zettlemoyer, Nicola Cancedda, and Thomas Scialom. Toolformer: Language models can teach themselves to use tools, 2023.

[6] Meta llama-2 models. <https://huggingface.co/models?sort=trending&search=meta+Llama-2>, 2024.

[7] Textsynth: Text completion. <https://textsynth.com/completion.html>.

[8] Openai: ChatGPT. <https://chat.openai.com/>, [Accessed in Aug. 2023].

[9] GitHub Copilot. <https://github.com/features/copilot/>, 2024.

[10] Speaking your language: The transformer in machine translation. <https://blog.huawei.com/2022/02/01/speaking-your-language-transformer-machine-translation/>.

[11] Elozino Egonmwan and Yllias Chali. Transformer-based model for single documents neural summarization. In *Proceedings of the 3rd Workshop on Neural Generation and Translation*, pages 70–79, Hong Kong, November 2019. Association for Computational Linguistics.

[12] Zi Gong, Cuiyun Gao, Yasheng Wang, Wenchao Gu, Yun Peng, and Zenglin Xu. Source code summarization with structural relative position guided transformer. In *2022 IEEE International Conference on Software Analysis, Evolution and Reengineering (SANER)*, pages 13–24, 2022.

[13] Haopeng Zhang, Xiao Liu, and Jiawei Zhang. HEGEL: Hypergraph transformer for long document summarization, 2022.

[14] Ashutosh Adhikari, Achyudh Ram, Raphael Tang, and Jimmy Lin. Docbert: BERT for document classification. *CoRR*, abs/1904.08398, 2019.

[15] Xiang Dai, Ilias Chalkidis, Sune Darkner, and Desmond Elliott. Revisiting transformer-based models for long document classification, 2022.

[16] Ashish Vaswani, Noam Shazeer, Niki Parmar, Jakob Uszkoreit, Llion Jones, Aidan N Gomez, Łukasz Kaiser, and Illia Polosukhin. Attention is all you need. In I. Guyon, U. Von Luxburg, S. Bengio, H. Wallach, R. Fergus, S. Vishwanathan, and R. Garnett, editors, *Advances in Neural Information Processing Systems*, volume 30. Curran Associates, Inc., 2017.

[17] Zhenyu Zhang, Ying Sheng, Tianyi Zhou, Tianlong Chen, Lianmin Zheng, Ruisi Cai, Zhao Song, Yuandong Tian, Christopher Ré, Clark Barrett, Zhangyang "Atlas" Wang, and Beidi Chen. H2o: Heavy-hitter oracle for efficient generative inference of large language models. In A. Oh, T. Neumann, A. Globerson, K. Saenko, M. Hardt, and S. Levine, editors, *Advances in Neural Information Processing Systems*, volume 36, pages 34661–34710. Curran Associates, Inc., 2023.

[18] Suyu Ge, Yunan Zhang, Liyuan Liu, Minjia Zhang, Jiawei Han, and Jianfeng Gao. Model tells you what to discard: Adaptive kv cache compression for llms. *arXiv preprint arXiv:2310.01801*, 2023.

[19] Zichang Liu, Aditya Desai, Fangshuo Liao, Weitao Wang, Victor Xie, Zhaozhuo Xu, Anastasios Kyrillidis, and Anshumali Shrivastava. Scissorhands: Exploiting the persistence of importance hypothesis for llm kv cache compression at test time. In A. Oh, T. Neumann, A. Globerson, K. Saenko, M. Hardt, and S. Levine, editors, *Advances in Neural Information Processing Systems*, volume 36, pages 52342–52364. Curran Associates, Inc., 2023.

[20] Dongjie Yang, XiaoDong Han, Yan Gao, Yao Hu, Shilin Zhang, and Hai Zhao. Pyramidinfer: Pyramid kv cache compression for high-throughput llm inference, 2024.

[21] Alessio Devoto, Yu Zhao, Simone Scardapane, and Pasquale Minervini. A simple and effective l_2 norm-based strategy for KV cache compression. In Yaser Al-Onaizan, Mohit Bansal, and Yun-Nung Chen, editors, *Proceedings of the 2024 Conference on Empirical Methods in Natural Language Processing*, pages 18476–18499, Miami, Florida, USA, November 2024. Association for Computational Linguistics.

[22] Muhammad Adnan, Akhil Arunkumar, Gaurav Jain, Prashant Nair, Ilya Soloveychik, and Purushotham Kamath. Keyformer: Kv cache reduction through key tokens selection for efficient generative inference. In P. Gibbons, G. Pekhimenko, and C. De Sa, editors, *Proceedings of Machine Learning and Systems*, volume 6, pages 114–127, 2024.

[23] Sotiris Anagnostidis, Dario Pavllo, Luca Biggio, Lorenzo Noci, Aurelien Lucchi, and Thomas Hofmann. Dynamic context pruning for efficient and interpretable autoregressive transformers. In A. Oh, T. Naumann, A. Globerson, K. Saenko, M. Hardt, and S. Levine, editors, *Advances in Neural Information Processing Systems*, volume 36, pages 65202–65223. Curran Associates, Inc., 2023.

[24] Wonbeom Lee, Jungi Lee, Junghwan Seo, and Jaewoong Sim. InfiniGen: Efficient generative inference of large language models with dynamic KV cache management. In *18th USENIX Symposium on Operating Systems Design and Implementation (OSDI 24)*, pages 155–172, Santa Clara, CA, July 2024. USENIX Association.

[25] Chaoran Zhang, Lixin Zou, Dan Luo, Min Tang, Xiangyang Luo, Zihao Li, and Chenliang Li. Efficient sparse attention needs adaptive token release, 2024.

[26] Huiqiang Jiang, YUCHENG LI, Chengruidong Zhang, Qianhui Wu, Xufang Luo, Surin Ahn, Zhenhua Han, Amir H. Abdi, Dongsheng Li, Chin-Yew Lin, Yuqing Yang, and Lili Qiu. MIInference 1.0: Accelerating pre-filling for long-context LLMs via dynamic sparse attention. In *The Thirty-eighth Annual Conference on Neural Information Processing Systems*, 2024.

[27] Yefei He, Luoming Zhang, Weijia Wu, Jing Liu, Hong Zhou, and Bohan Zhuang. Zipcache: Accurate and efficient kv cache quantization with salient token identification, 2024.

[28] Hao Kang, Qingru Zhang, Souvik Kundu, Geonhwa Jeong, Zaoxing Liu, Tushar Krishna, and Tuo Zhao. GEAR: An efficient KV cache compression recipe for near-lossless generative inference of LLM. *arXiv preprint arXiv:2403.05527*, 2024.

[29] Zirui Liu, Jiayi Yuan, Hongye Jin, Shaochen Zhong, Zhaozhuo Xu, Vladimir Braverman, Beidi Chen, and Xia Hu. KIVI: A tuning-free asymmetric 2bit quantization for KV cache. In Ruslan Salakhutdinov, Zico Kolter, Katherine Heller, Adrian Weller, Nuria Oliver, Jonathan Scarlett, and Felix Berkenkamp, editors, *Proceedings of the 41st International Conference on Machine Learning*, volume 235 of *Proceedings of Machine Learning Research*, pages 32332–32344. PMLR, 21–27 Jul 2024.

[30] Yuhang Liu, Hanchen Li, Yihua Cheng, Siddhant Ray, Yuyang Huang, Qizheng Zhang, Kuntai Du, Jiayi Yao, Shan Lu, Ganesh Ananthanarayanan, Michael Maire, Henry Hoffmann, Ari Holtzman, and Junchen Jiang. Cachegen: Kv cache compression and streaming for fast large language model serving. In *Proceedings of the ACM SIGCOMM 2024 Conference*, ACM SIGCOMM '24, page 38–56, New York, NY, USA, 2024. Association for Computing Machinery.

[31] Coleman Hooper, Sehoon Kim, Hiva Mohammadzadeh, Michael W. Mahoney, Yakun Sophia Shao, Kurt Keutzer, and Amir Gholami. Kvquant: Towards 10 million context length llm inference with kv cache quantization, 2024.

[32] V. Klema and A. Laub. The singular value decomposition: Its computation and some applications. *IEEE Transactions on Automatic Control*, 25(2):164–176, 1980.

[33] ZeroC code. <https://anonymous.4open.science/r/ZeroC>, 2024.

[34] Singular value decomposition solver from scipy. <https://docs.scipy.org/doc/scipy/reference/generated/scipy.linalg.svd.html>, 2024.

[35] Genre classification dataset imdb. <https://www.kaggle.com/datasets/hijest/genre-classification-dataset-imdb>.

[36] arxiv. <https://arxiv.org>.

[37] Sunhao Dai, Weihao Liu, Yuqi Zhou, Liang Pang, Rongju Ruan, Gang Wang, Zhenhua Dong, Jun Xu, and Ji-Rong Wen. Cocktail: A comprehensive information retrieval benchmark with llm-generated documents integration, 2024.

[38] Mark Chen, Jerry Tworek, Heewoo Jun, Qiming Yuan, Henrique Ponde de Oliveira Pinto, Jared Kaplan, Harri Edwards, Yuri Burda, Nicholas Joseph, Greg Brockman, Alex Ray, Raul Puri, Gretchen Krueger, Michael Petrov, Heidy Khlaaf, Girish Sastry, Pamela Mishkin, Brooke Chan, Scott Gray, Nick Ryder, Mikhail Pavlov, Alethea Power, Lukasz Kaiser, Mohammad Bavarian,

Clemens Winter, Philippe Tillet, Felipe Petroski Such, Dave Cummings, Matthias Plappert, Fotios Chantzis, Elizabeth Barnes, Ariel Herbert-Voss, William Hebgen Guss, Alex Nichol, Alex Paino, Nikolas Tezak, Jie Tang, Igor Babuschkin, Suchir Balaji, Shantanu Jain, William Saunders, Christopher Hesse, Andrew N. Carr, Jan Leike, Josh Achiam, Vedant Misra, Evan Morikawa, Alec Radford, Matthew Knight, Miles Brundage, Mira Murati, Katie Mayer, Peter Welinder, Bob McGrew, Dario Amodei, Sam McCandlish, Ilya Sutskever, and Wojciech Zaremba. Evaluating large language models trained on code, 2021.

[39] Meta Llama-3.1. <https://llama.meta.com/>, 2024.

[40] 01-ai model Yi. <https://huggingface.co/01-ai/Yi-34B-200K>, 2024.

[41] Mistral-v0.3. <https://huggingface.co/mistralai/Mistral-7B-Instruct-v0.3>, 2024.

[42] Microsoft Phi-3. <https://huggingface.co/microsoft/Phi-3-medium-128k-instruct>, 2024.

[43] Falcon-180b. <https://huggingface.co/tiiuae/falcon-180B>, 2024.

[44] Amey Agrawal, Nitin Kedia, Ashish Panwar, Jayashree Mohan, Nipun Kwatra, Bhargav Gulavani, Alexey Tumanov, and Ramachandran Ramjee. Taming Throughput-Latency tradeoff in LLM inference with Sarathi-Serve. In *18th USENIX Symposium on Operating Systems Design and Implementation (OSDI 24)*, pages 117–134, Santa Clara, CA, July 2024. USENIX Association.

[45] Yinmin Zhong, Shengyu Liu, Junda Chen, Jianbo Hu, Yibo Zhu, Xuanzhe Liu, Xin Jin, and Hao Zhang. Dist-Serve: Disaggregating prefill and decoding for goodput-optimized large language model serving. In *18th USENIX Symposium on Operating Systems Design and Implementation (OSDI 24)*, pages 193–210, Santa Clara, CA, July 2024. USENIX Association.

[46] Amazon EC2 P4 instances. <https://aws.amazon.com/ec2/instance-types/p4/>.

[47] Connor Holmes, Masahiro Tanaka, Michael Wyatt, Ammar Ahmad Awan, Jeff Rasley, Samyam Rajbhandari, Reza Yazdani Aminabadi, Heyang Qin, Arash Bakhtiari, Lev Kurilenko, and Yuxiong He. Deepspeed-fastgen: High-throughput text generation for llms via mii and deepspeed-inference. *arXiv preprint arXiv:2401.08671*, 2024.

[48] Woosuk Kwon, Zhuohan Li, Siyuan Zhuang, Ying Sheng, Lianmin Zheng, Cody Hao Yu, Joseph Gonzalez, Hao Zhang, and Ion Stoica. Efficient memory management for large language model serving with page-dattention. In *Proceedings of the 29th Symposium on Operating Systems Principles, SOSP ’23*, page 611–626, New York, NY, USA, 2023. Association for Computing Machinery.

[49] Pratyush Patel, Esha Choukse, Chaojie Zhang, Aashaka Shah, Íñigo Goiri, Saeed Maleki, and Ricardo Bianchini. Splitwise: Efficient generative llm inference using phase splitting. In *2024 ACM/IEEE 51st Annual International Symposium on Computer Architecture (ISCA)*, pages 118–132, 2024.

[50] Hello GPT-4o. <https://openai.com/index/hello-gpt-4o/>, 2024.

[51] Jianlin Su, Murtadha Ahmed, Yu Lu, Shengfeng Pan, Wen Bo, and Yunfeng Liu. Roformer: Enhanced transformer with rotary position embedding. *Neurocomput.*, 568(C), March 2024.

[52] Tri Dao. Flashattention-2: Faster attention with better parallelism and work partitioning, 2023.

[53] NVIDIA CUTLASS. <https://github.com/NVIDIA/cutlass>.

[54] Quart. <https://quart.palletsprojects.com/en/latest/>.

[55] Rongzhi Zhang, Kuang Wang, Liyuan Liu, Shuohang Wang, Hao Cheng, Chao Zhang, and Yelong Shen. Lorc: Low-rank compression for llms kv cache with a progressive compression strategy, 2024.

[56] Chi-Chih Chang, Wei-Cheng Lin, Chien-Yu Lin, Chong-Yan Chen, Yu-Fang Hu, Pei-Shuo Wang, Ning-Chi Huang, Luis Ceze, Mohamed S. Abdelfattah, and Kai-Chiang Wu. Palu: Compressing kv-cache with low-rank projection, 2024.